




## Research

# Silencing of SCEL promotes progression of oral squamous cell carcinoma via activating TGF- $\beta$ /Smad pathway

Danping Li<sup>1,2</sup> · Limei Li<sup>1,2</sup> · Shu Wu<sup>1,2</sup> · Jun Zhao<sup>1,2</sup> · Haishan Zhang<sup>1,2</sup> · Qiaoli Chen<sup>1,2</sup> · Yingxi Mo<sup>3</sup> · Liudmila Matskova<sup>4,6</sup> · Ping Li<sup>1</sup>  · Xiaoying Zhou<sup>2,5</sup> 

Received: 7 November 2024 / Accepted: 17 April 2025

Published online: 15 May 2025

© The Author(s) 2025 

## Abstract

**Objective** SCEL serves as a precursor protein for the cornified envelope (CE), and its abnormal expression has been identified in various malignancies. Despite this, the functional role and detailed mechanisms of SCEL in oral squamous cell carcinoma (OSCC) remain to be clarified.

**Methods** mRNA and protein expression of SCEL in OSCC cell lines and patient tissues were examined by qRT-PCR and IHC. In vitro and in vivo experiments assessed SCEL's influence on proliferation, apoptosis, cell cycle, ROS production, migration, and invasion. Western blotting was used to analyze SCEL's effect on various signaling pathways, and a dual-luciferase reporter assay identified the miRNA that targets SCEL.

**Results** SCEL is downregulated in OSCC, which correlates with reduced tumor cell differentiation and lymph node metastasis. SCEL inhibits OSCC proliferation, induces cell cycle arrest, apoptosis, and ROS production. SCEL suppresses the TGF- $\beta$ /Smad pathway, inhibiting migration and invasion. SCEL also triggers MET and downregulates VEGFC, reducing lymph node metastasis probability. miR-5696 inhibitor effectively inhibits OSCC proliferation and invasion by targeting SCEL.

**Conclusion** SCEL acts as a tumor suppressor in OSCC, influencing its progression and potential metastasis. Loss of SCEL facilitates OSCC progression by activating TGF- $\beta$ /Smad signaling. Upregulating SCEL and silencing miR-5696 hold therapeutic promise for OSCC.

**Keywords** Oral squamous cell carcinoma · SCEL · TGF- $\beta$  signaling pathway · Differentiation · Metastasis · MiR-5696

## Abbreviations

AUC            The area under the curve  
CE            Cornified envelope

Danping Li and Limei Li have contributed equally to this work.

**Supplementary Information** The online version contains supplementary material available at <https://doi.org/10.1007/s12672-025-02423-4>.

✉ Ping Li, [liping@gxmu.edu.cn](mailto:liping@gxmu.edu.cn); ✉ Xiaoying Zhou, [zhouxiaoying1982@foxmail.com](mailto:zhouxiaoying1982@foxmail.com) | <sup>1</sup>Department of Pathology, College & Hospital of Stomatology, Guangxi Medical University, #10 Shuangyong Road, Nanning 530021, China. <sup>2</sup>Ministry of Education, Key Laboratory of High-Incidence-Tumor Prevention & Treatment (Guangxi Medical University), Nanning, China. <sup>3</sup>Department of Pathology, Guangxi Medical University Cancer Hospital, Nanning, China. <sup>4</sup>Department of Microbiology, Tumor and Cell Biology, Karolinska Institutet, 17177 Stockholm, Sweden. <sup>5</sup>Life Science Institute, Guangxi Medical University, #22 Shuangyong Road, Nanning 530021, China. <sup>6</sup>Institute of Molecular Biology and Biophysics of Federal Research Center of Fundamental and Translational Medicine (IMBB FRC FTM), 2/12, Timakova Street, 630117 Novosibirsk, Russia.



CRC	Colorectal cancer
CDDP	Cisplatin
EMT	Epithelial-mesenchymal transition
FBS	Fetal bovine serum
HNSCC	Head and neck squamous cell carcinoma
IHC	Immunohistochemical
LIM	LIN-11, Isl1, and MEC-3
LYVE1	Lymphatic Vessel Endothelial Hyaluronan Receptor 1
MFI	Mean fluorescence intensity
OSCC	Oral squamous cell carcinoma
PVDF	Polyvinylidene fluoride
ROC curve	The receiver operating characteristic curve
SCEL	Sciellin
HRP	Standard deviation horseradish peroxidase
TCGA	The Cancer Genome Atlas
TGF- $\beta$ 1	Transforming growth factor $\beta$ 1
VEGFC	Vascular endothelial growth factor/vascular endothelial growth factor C
WB	Western blotting

## 1 Introduction

Oral cancer originates from the oral epithelium and is the most common malignant tumor in the maxillofacial region [1]. In 2020, there were 377,713 new cases diagnosed, and 177,757 deaths [2]. Among the different types of oral cancer, oral squamous cell carcinoma (OSCC) is the most common, accounting for 90% of oral cancer cases [3]. OSCC is characterized by invasiveness and early lymph node metastasis. More importantly, these metastases often lack distinct clinical and radiological findings. The combination of these factors leads to frequent local recurrence [4]. Despite a combination of therapies including surgery, chemotherapy, radiotherapy, and targeted therapy [5], OSCC remains a fatal disease with a five-year survival rate of only 50%, in addition to causing severe deformities and reducing the patient's quality of life [6]. Therefore, it is urgent to develop novel approaches for early diagnosis and prognosis.

SCEL is localized on human chromosome 13q22 and encodes a distinctive 75.3 kDa protein, characterized by internal repeats rich in Lys and Gln residues, along with a LIM (LIN-11, Isl1, and MEC-3) domain [7]. SCEL serves as a precursor protein for the cornified envelope (CE) and plays a crucial role in epithelial barrier formation cell differentiation and intercellular adhesion [8]. SCEL protein is strongly expressed in the squamous epithelium of the oral cavity, esophagus, and vagina [7]. In colorectal cancer and gallbladder carcinoma, SCEL expression is transcriptionally repressed [9, 10], and studies have shown that SCEL can inhibit the migration of colorectal cancer cells and counteract the activity of transforming growth factor  $\beta$  1 (TGF- $\beta$ 1) [9]. TGF- $\beta$ 1 is a pleiotropic cytokine that exerts its effects by activating the TGF- $\beta$ /Smad signaling pathway. In cancer, the TGF- $\beta$ /Smad signaling pathway not only promotes tumor cell proliferation and survival but also plays a critical role in the epithelial-mesenchymal transition (EMT), a process that is essential for cancer cells to acquire invasive and migratory capabilities [11].

SCEL has been identified as significantly downregulated in tongue squamous cell carcinoma tissues through genome-wide studies [12]. However, its specific biological functions and molecular mechanisms in OSCC remain unclear. This study investigates the expression pattern of SCEL in OSCC and its relationship with clinicopathological characteristics. Additionally, we examined the role of SCEL in regulating the biological behavior of OSCC cells and its potential molecular mechanisms, aiming to evaluate its potential as a diagnostic and therapeutic target.

## 2 Materials and methods

### 2.1 Bioinformatic analysis based on The cancer genome atlas (TCGA) database

TCGA datasets of head and neck squamous cell carcinoma (HNSCC) were retrieved and downloaded from the Xena resource (<http://xena.ucsc.edu/>), including mRNA information and corresponding clinical parameters. Specimens from all

oral-related areas, including the alveolar ridge, buccal mucosa, mouth floor, tongue, lip, and hard palate, were screened out [13]. Incomplete data on mRNA expression and clinical parameters were eliminated.

## 2.2 Cell lines and human tissues samples

HOEC, a normal oral epithelial cell line immortalized by HPV16 E6/E7, and the tongue OSCC cell lines CAL27 and SAS, were maintained by the Key Laboratory of High-Incidence-Tumor Prevention & Treatment (Guangxi Medical University). All cell lines were authenticated using STR profiling and confirmed mycoplasma-negative. All cell lines were cultured in DMEM medium with 10% fetal bovine serum (FBS) (Sigma, USA) and 1% penicillin–streptomycin (Sigma, USA) [14]. The cells were incubated at 37 °C with 5% CO<sub>2</sub> and in a humidified atmosphere.

Forty freshly excised OSCC tissue samples and 40 adjacent non-cancerous tissues were collected from the Department of Pathology, Affiliated Stomatological Hospital of Guangxi Medical University. Additionally, a total of 76 paraffin-embedded cancer tissues and 76 adjacent non-cancerous tissues were also collected from the same department between 2019 and 2022. The non-cancerous tissues were obtained from areas located at least 5 cm away from the tumor margin.

## 2.3 RT-qPCR assay

Total RNA from cells and fresh tissues was extracted using Trizol reagent (Invitrogen, USA). Subsequently, cDNA was synthesized using a one-step RNA-to-DNA kit (TransGen Biotech, China). RT-qPCR was conducted on the StepOnePlusQ5 system (Thermo Fisher Scientific Company, USA). GAPDH was chosen as the internal reference. The relative gene expression level was calculated using the  $2^{-\Delta\Delta CT}$  method. All experiments were conducted in triplicate. The primer sequences used in this study were as follows: for SCEL, the upstream primer was 5'-CGAGCAGAAGAAGTGAAGACCT-3', and the downstream primer was 5'-ATTATCAAGGCTCTGGCCCC-3'. For VEGFC, the upstream primer was 5'-GGGGAAGGAGTTTGGAGTCG-3', and the downstream primer was 5'-GCTGGCAGGGAACGTCTAAT-3'. For GAPDH, the upstream primer was 5'-GCTCAGACACCATGGGGAAG-3', and the downstream primer was 5'-TGAGTTGAGGTCAATGAAGGGG-3'. All primers were designed by Primer-BLAST and synthesized by Sangon Biotech (Shanghai, China).

## 2.4 Immunohistochemical (IHC) staining

The tissue paraffin sections were dewaxed in xylene and hydrated. Antigen retrieval was performed using EDTA repair solution and cooled. Sections were treated with peroxidase blocking enzyme and incubated with primary antibody overnight, followed by HRP (horseradish peroxidase)-labeled secondary antibody. Sections were stained with DAB, counterstained with hematoxylin, differentiated in hydrochloric acid, and neutralized in lithium carbonate. Finally, sections were dehydrated, cleared in xylene, and sealed with neutral resin. Positive and negative controls were included. Immunohistochemical staining results were evaluated by two pathologists independently. The details of primary antibodies are provided in the Appendix 1.

Semi-quantitative analysis determined protein expression based on staining intensity and positive cell areas. OSCC cells and/or normal oral squamous cells were observed under low (100 ×) and high (400 ×) power magnification. Ten fields were randomly selected. Staining intensity was categorized as negative or trace (0), weak (1), moderate (2), and strong (3). The percentage of positive tumor cells indicated the proportion of cells showing positive staining for a specific marker, such as SCEL, ranging from 0 to 100%. The final protein expression score (0–300) was calculated by multiplying these two results and averaging them [15]. The cut-off value for the H-score, determined by ROC analysis, divided patients into high expression (H score ≥ 105) and low expression groups (H score < 105) [16].

## 2.5 The receiver operating characteristic curve analysis

The receiver operating characteristic curve (ROC curve) was used to measure the sensitivity and specificity of SCEL in the diagnosis of OSCC. Additionally, the area under the curve (AUC) was utilized to determine the diagnostic value of SCEL expression. Moreover, the Youden index was used to determine the optimal critical value of SCEL expression.

## 2.6 Cell transfection

Transfection was performed with Lipofectamine 3000® Reagent (Thermo Fisher Scientific, USA) according to the manufacturer's instructions. OSCC cell lines were transfected with plasmids while an empty vector was used as control (pCMV6). Transfection efficiency was confirmed by qRT-PCR and immunoblotting analysis 48 h after transfection.

## 2.7 Western blot analysis

Proteins were extracted with RIPA buffer (Sigma, USA) and quantified using a bicinchoninic acid protein assay kit (Beyotime, China). Equal amounts of protein were separated by SDS-PAGE (Invitrogen, USA) and transferred to PVDF membranes (Millipore, USA). Membranes were blocked with 5% skimmed milk, incubated overnight with primary antibodies, then washed with TBST. After incubation with fluorescent secondary antibodies for 90 min, membranes were re-washed and visualized using the LI-COR Odyssey Infrared Imaging System. GAPDH served as a loading control. The details of primary antibodies are provided in the Appendix 1.

## 2.8 Cell proliferation assay

Proliferation was determined using a CCK8 assay. The cells were seeded at a density of  $1 \times 10^3$  cells per well in 96-well plates and cultured in a cell incubator. On days 1, 2, 3, 4, and 5, 10  $\mu$ l of CCK8 solution (Dongren Chemical Technology, China) was added to each well. After incubation for 2 h, the absorbance at 450 nm was measured using a microplate reader (BioTek, Vermont, USA).

## 2.9 Colony formation assay

Colony formation assay was conducted using a 6-well plate. 500 cells were seeded to each well in 2 mL of medium. After continuous culture for 14 days, cells were washed three times with PBS, fixed with 4% paraformaldehyde for 30 min, and stained with 0.1% crystal violet for 30 min. The number of colony-forming units (CFUs), consisting of more than 10 cells, were counted under a microscope.

## 2.10 Tumorigenesis experiment in nude mice

The male nude mice were divided into two groups, each comprising 4 mice. One group was administered SAS cells transfected with the SCEL gene, while the other group received cells with an empty vector. Approximately  $1 \times 10^7$  cells were injected into the armpits of the mice. The volume of the nodules was measured every 3 days. Upon the observation of visible nodules and exceeding an ethical limit, the mice were euthanized by CO<sub>2</sub> inhalation, and the tumors were photographed and weighed. IHC analysis was conducted to assess the expression of the SCEL gene.

## 2.11 Cell apoptosis assay

Apoptosis was assessed using a commonly used apoptosis kit (AP105, MultiSciences, China). After 48 h of plasmid transfection, cells were digested with trypsin-EDTA, and a total of  $3 \times 10^6$  cells (including those in the supernatant) were collected. The cells were then washed twice with ice-cold PBS and resuspended in a suitable volume of pre-cooled  $1 \times$  Binding Buffer. Each tube was then incubated with 5  $\mu$ l of Annexin V APC and 10  $\mu$ l of 7 AAD. The mixture was gently vortexed and incubated at room temperature in the dark for 5 min. The stained cells were analyzed using a flow cytometer (BD Biosciences, San Diego, CA, USA), with at least 10,000 events recorded. Cell populations in different quadrants were measured by quadrant statistics.

## 2.12 Cell cycle analysis

Cell cycle progression was assessed using a Cell Cycle Detection Kit (CCS012, MultiSciences, China) following the manufacturer's instructions. After 48 h of plasmid transfection,  $3 \times 10^6$  cells were collected and 2 mL of anhydrous



ethanol was added dropwise to the cell pellet while vortexing, then incubated overnight at  $-20^{\circ}\text{C}$ . The next day, the cells were resuspended in 1 mL of PBS and allowed to rehydrate for 15 min. Then, 500–1000  $\mu\text{L}$  of DNA Staining Solution was added, and the mixture was gently vortexed for 5–10 s to mix well. The cells were incubated at room temperature in the dark for 30 min. Ensure thorough vortexing and use the lowest sample loading speed for detection on the flow cytometer. At least 10,000 cells were recorded.

### 2.13 Detection of reactive oxygen species (ROS)

OSCC cells were incubated with 10  $\mu\text{M}$  DCFH-DA (Solebao, CA1410) at  $37^{\circ}\text{C}$  for 20 min in the dark. After incubation, cells were washed three times with fresh culture medium and subjected to various detection methods. ROS levels were measured at an excitation wavelength of 488 nm and an emission wavelength of 525 nm. For flow cytometry,  $1 \times 10^6$  cells were resuspended in 500  $\mu\text{L}$  of fresh culture medium and analyzed using a flow cytometer (BD Biosciences). For confocal microscopy,  $1 \times 10^5$  cells were seeded in 15 mm confocal dishes and visualized using a confocal laser scanning microscope (Leica Microsystems). For the microplate reader assay, 3,000 cells per well were added to a black plate. Fluorescence intensity was measured using a TECAN Infinite® 200 PRO microplate reader.

### 2.14 Wound healing assay

Wound healing assays were performed using silicone culture inserts (Ibidi, Germany) with two adjacent wells to create a wound closure seeding model.  $5 \times 10^4$  cells were seeded into each well and cultured to form a confluent monolayer. The wound was created by carefully removing the silicone inserts. The remaining cells were incubated with 0.5% FBS medium. The cells were observed under an inverted microscope (Olympus, Japan), and images were acquired immediately after wounding and at 6-h intervals (200 $\times$  magnification). The wound healing rates were calculated using ImageJ.

### 2.15 Transwell invasion assay

Transwell invasion assays were conducted using 24-well transwell chambers with 8.0  $\mu\text{m}$  pore size inserts (Corning, 3422). Matrigel (Corning, USA, 354,234) was diluted with FBS-free medium (1: 29). The upper chamber was coated with a total of 100  $\mu\text{L}$  above mixture and incubated for 4 h.  $8 \times 10^4$  cells were seeded into the upper chamber in 200  $\mu\text{L}$  of FBS-free medium, while 800  $\mu\text{L}$  medium with 20% FBS was added to the bottom chamber. After incubation for 24 h, the cells were fixed with 4% paraformaldehyde for 30 min and stained with crystal violet for an additional 30 min. The number of cells that had invaded the Matrigel was counted using an inverted microscope (Olympus, Japan) in at least 5 random fields (400 $\times$  magnification).

### 2.16 Cells viability assay

Cells were transfected with SCEL, seeded into 96-well plates at 3000 cells per well, and incubated overnight. The cells were then treated with various concentrations of cisplatin (CDDP, MCEHY-17394) (0, 0.5, 1, 2, 4, 8, 16, 32, and 64  $\mu\text{M}$ ) for 24 h. Subsequently, 10  $\mu\text{L}$  of CCK8 solution was added to each well and incubated for 2 h. The absorbance at 450 nm was measured using a microplate reader.

### 2.17 miRNA prediction and binding site analysis

Micro-CDS, miRDB, TargetScan, and Targets were used to predict miRNAs which potentially target SCEL. The resulting intersection of predicted miRNAs from these tools was further analyzed. Specifically, the binding site of has-miR-5696 on SCEL was predicted using miRDB.

### 2.18 miRNA expression analysis

Total RNA was reverse transcribed using the MirX™ miRNA First-Strand Synthesis kit (Takara 638,313). Expression levels of has-miR-5696 were quantified through qRT-PCR using the TB Green Advantage qPCR Premix (Takara 639,676). The primer sequence for has-miR-5696 (forward primer) is: GCTCATTTAAGTAGTCTGATGCCA. The reverse primer used was

**Fig. 1** Expression patterns, clinical significance, and diagnostic potential of SCEL in OSCC. **A** SCEL mRNA level in OSCC tissues (n = 343) and normal control samples (n = 32) based on the TCGA database. **B, C** The transcription level of SCEL in OSCC cell lines and in the normal oral epithelial cell line HOEC was detected by qRT-PCR. The same approach was applied in OSCC tissues (n = 40) and matched non-cancerous tissues. **D** Representative images of IHC staining of SCEL protein in OSCC and adjacent tissues. **E** Comparison of SCEL protein expression levels between OSCC (n = 76) and adjacent non-cancerous tissues (n = 76) using the H-score from immunohistochemical staining. **F** Representative images of IHC staining of SCEL and P63 proteins in OSCC tissues with well (n = 18), moderate (n = 16), and poor differentiation (n = 14). **G** Comparison of SCEL and P63 in OSCC tissues with different differentiation. **H** Representative images of IHC staining of SCEL and VEGFC proteins in normal oral mucosa (n = 20), dysplastic oral mucosa (n = 14), OSCC tissues (n = 54), and lymphatic node metastatic carcinoma (n = 39). **I** Comparison of SCEL and VEGFC in different pathological tissues. **J** ROC curve of SCEL mRNA levels in OSCC in TCGA database. **K** ROC curve of SCEL protein levels in OSCC

mRQ 3. U6 snRNA (primer sequences: Forward: CTCGCTTCGGCAGCACAT, Reverse: TTTGCGTGTCATCCTTGCG) was used as a control for the ddCt method.

## 2.19 Transfection with miRNA mimics and inhibitors

Transfection was performed with Lipofectamine 3000<sup>®</sup> Reagent (Thermo Fisher Scientific, USA) according to the manufacturer's instructions. OSCC cell lines were transfected with miR-5696 mimics or inhibitors. The sequences used for transfection are as follows: hsa-miR-5696 mimics sense: CTCATTTAAGTAGTCTGATGCC, hsa-miR-5696 mimics antisense: GGCATCAGACTACTTAAATGAG, hsa-miR-5696 inhibitor: GGCATCAGACTACTTAAATGAG, Mimics-NC and inhibitor-NC were used as negative controls. Transfection efficiency was confirmed by qRT-PCR and western blot analysis 48 h after transfection.

### 2.19.1 Dual-luciferase reporter assay

The dual-luciferase reporter assay was performed using 293 T cells and the TransDetect<sup>®</sup> Double-Luciferase Reporter Assay Kit (TransGen Biotech, FR201). Cells were washed twice with PBS and lysed with 1 × lysis buffer at room temperature for 10 min. Lysates were then centrifuged at 12,000 ×g for 10 min at 2–8 °C, and the supernatant was collected. For the assay, 100 µl of Luciferase Reaction Reagent was added to the wells, followed by 20 µl of cell lysate. Firefly luciferase activity was measured using a luminometer. Subsequently, 100 µl of Luciferase Reaction Reagent II was added to the wells, and Renilla luciferase activity was measured.

## 2.20 Statistical analysis

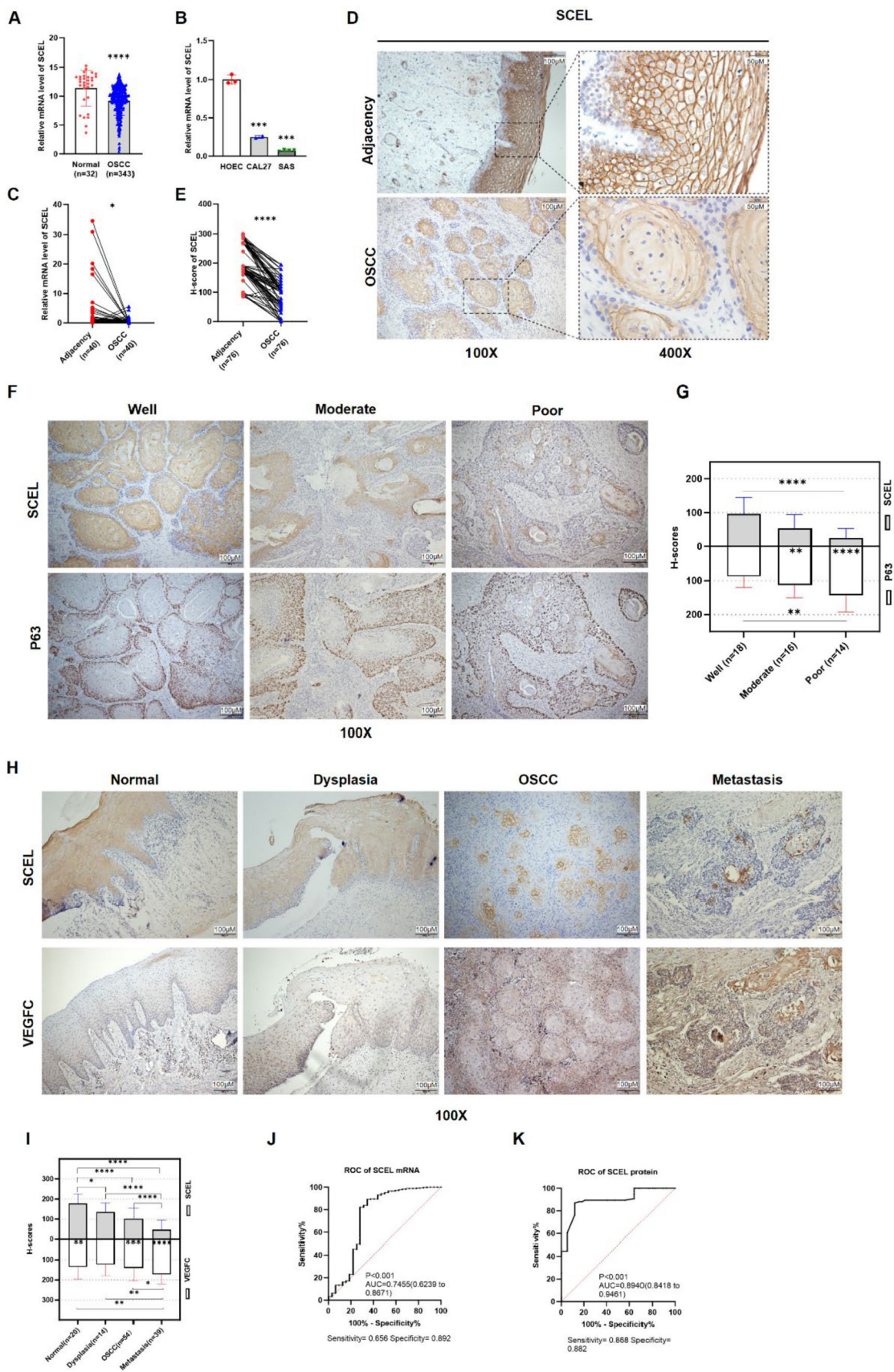
Continuous variables were presented as means ± standard deviation (SD) and were compared using two-tailed t-tests and one-way ANOVA. Categorical variables were presented as frequencies and analyzed using the  $\chi^2$  test. Pearson correlation analysis was performed to assess the association among continuous variables. The diagnostic value for the SCEL level was assessed using ROC curve analysis.  $P < 0.05$  was considered statistically significant. Statistical analysis was performed using Prism 9.0 (GraphPad Software, USA) and SPSS version 25.0 (SPSS, USA). \* $P < 0.05$ , \*\* $P < 0.01$ , \*\*\* $P < 0.001$ , and \*\*\*\* $P < 0.0001$ .

## 3 Results

### 3.1 SCEL is significantly downregulated in OSCC

We initially identified 343 OSCC specimens and 32 normal oral specimens from the TCGA database for bioinformatics analysis. Upon analyzing the gene expression data, we observed a significant decrease in SCEL mRNA levels in OSCC tissues compared to normal oral mucosa tissues (Fig. 1A,  $P < 0.0001$ , Appendix 2 ). Subsequent qRT-PCR analysis demonstrated a substantial downregulation of SCEL expression in OSCC cell lines (CAL27 and SAS) and in 40 freshly resected OSCC tissue samples when compared to the normal oral epithelial cell line (HOEC) and non-cancerous tissues, respectively (Fig. 1B, C, both  $P < 0.05$ ).

In addition, we examined the protein level of SCEL in 76 paraffin-embedded human OSCC and corresponding adjacent tissues using IHC staining. Figure 1D illustrates the predominant localization of SCEL on the cell membrane. The most intense staining observed in the keratinized layer (appearing as dark yellow or yellowish brown). In contrast, SCEL



staining in OSCC tissues appeared predominantly faint and concentrated in the center of the cancer nests. Paired-sample analysis revealed a significantly lower H-score of SCEL in the 76 OSCC specimens compared to adjacent non-cancerous specimens, with median H-scores of 105 (range: 0–195) and 190 (range: 85–300), respectively (Fig. 1E,  $P < 0.0001$ ). These findings provide further evidence supporting the downregulation of SCEL expression in OSCC.

### 3.2 Lower expression of SCEL correlated with poor tumor differentiation and lymph node metastasis in OSCC

We further analyzed the correlation between SCEL protein expression level and various clinical characteristics of OSCC, including age, gender, pathological stage, TNM stage and maximum tumor diameter. Our analysis revealed a significant association between SCEL expression and tumor differentiation, TNM stage, and N stage in OSCC. These findings suggest that SCEL expression may play a role in tumor differentiation and lymph node metastasis in patients. However, the unequal sample sizes warrant further studies with more balanced groups to validate these observations. No significant associations were found between SCEL expression and age, sex, tumor stage, or tumor size (Table 1).

P63, a transcription factor essential for epithelial cell differentiation, is commonly used as a marker for identifying basal cells [17]. To validate the association between SCEL expression and OSCC cell differentiation, we investigated the concurrent expression of SCEL and P63 proteins in OSCC samples exhibiting high, moderate, and low levels of differentiation. IHC results revealed that SCEL and P63 proteins exhibited complementary expression patterns within the same cells. SCEL was abundantly expressed in well-differentiated OSCC tissues, where it localized to the cell membrane and cytoplasm, while its presence was almost negligible in poorly differentiated samples. Conversely, P63 was predominantly expressed in the nuclei of poorly differentiated OSCC cells, with significantly lower expression in well-differentiated samples (Fig. 1F). The expression of SCEL and P63 in OSCC samples with varying differentiation levels showed statistically

**Table 1** Correlation of SCEL expression to clinicopathological features in OSCC

Clinicopathological features	Lower expression (n = 54)	High expression (n = 52)	$\chi^2$	P
Gender			0.585	0.444
Male	38	40		
Female	16	12		
Age (years)			1.359	0.244
< 58	24	29		
≥ 58	30	23		
Tumor differentiation			24.770	< 0.0001***
Poorly differentiated	20	4		
Moderately differentiated	18	8		
Well differentiated	16	40		
TNM stage			10.262	0.016*
Stage I	9	10		
Stage II	10	15		
Stage III	22	7		
Stage IV	13	20		
T				
T1–T2	30	32	0.391	0.532
T3–T4	24	20		
N			6.400	0.011*
N0	21	33		
N1–N3	33	19		
Maximum tumor diameter (cm)			0.354	0.552
< 3	27	23		
≥ 3	27	29		

OSCC indicates oral squamous cell carcinoma

\*indicates that the comparison between groups is statistically significant, \* $P < 0.05$ , \*\*\* $P < 0.001$



significant differences (Fig. 1G,  $P < 0.0001$ ,  $P < 0.01$ , respectively). Paired-sample analysis indicated an inverse correlation between SCEL and P63 expressions in moderately and poorly differentiated OSCC tissues (Fig. 1G,  $P < 0.01$  and  $P < 0.0001$ , respectively). Statistical analysis revealed a significant correlation between P63 expression and both tumor differentiation and N stage in OSCC (Table 2,  $P < 0.05$ ). These findings suggest that as OSCC becomes less differentiated, P63 expression increases while SCEL expression decreases.

Vascular endothelial growth factor C (VEGFC), a member of the VEGF family, plays a crucial role in embryonic development, lymphatic vessel formation. It also serves as a marker for lymph node metastasis in squamous cell carcinoma [18]. To further confirm the close association of SCEL expression with OSCC progression, we validated the SCEL and VEGFC protein expression in the same set of samples, including normal oral mucosa, abnormal hyperplasia tissues, OSCC primary tumor, and carcinoma tissues from lymph node metastases. SCEL was strongly positive throughout the normal oral mucosa, particularly in the keratinized layer. In abnormal hyperplasia tissues, SCEL expression was present but mainly concentrated in the keratinized and granular layers. In OSCC tissues, SCEL staining was moderate to weak, with strong staining only in the center of the carcinoma nests. In carcinoma tissues from lymph node metastases, SCEL expression was weak (Fig. 1H). Conversely, VEGFC staining was stronger in OSCC and its metastatic tissues, while it was weaker in normal oral mucosa and abnormal hyperplasia tissues (Fig. 1H). Statistical analysis of SCEL and VEGFC expression in samples with varying levels of OSCC progression further supported this observation. Significant differences in SCEL protein expression were observed between the following groups: normal vs. abnormal, normal vs. OSCC, normal vs. lymph node metastasis, abnormal vs. lymph node metastasis, and OSCC vs. lymph node metastasis (Fig. 1I, all  $P < 0.05$ ). Meanwhile, VEGFC expression showed significant differences between normal and lymph node metastasis, abnormal and lymph node metastasis, and OSCC and lymph node metastasis (Fig. 1I, all  $P < 0.05$ ). Paired analysis showed that SCEL and VEGFC protein expressions were inversely correlated in normal tissues, OSCC tissues, and metastatic tissues (Fig. 1I,  $P < 0.01$ ,  $P < 0.001$  and  $P < 0.0001$  respectively).

**Table 2** Correlation of P63 expression to clinicopathological features in OSCC

Clinicopathological features	Lower expression (n = 18)	high expression (n = 24)	$\chi^2$	P
Gender			2.705	0.100
Male	12	22		
Female	6	2		
Age (years)			1.556	0.212
< 57	7	14		
≥ 57	11	10		
Tumor differentiation			8.215	0.016*
Poorly differentiated	2	10		
Moderately differentiated	6	10		
Well differentiated	10	4		
TNM stage			3.662	0.300
Stage I	3	4		
Stage II	6	4		
Stage III	3	10		
Stage IV	6	6		
T				
T1–T2	7	16	3.204	0.073
T3–T4	11	8		
N			4.582	0.032*
N0	12	8		
N1–N3	6	16		
Maximum tumor diameter (cm)			1.354	0.245
< 3	10	9		
≥ 3	8	15		

OSCC indicates oral squamous cell carcinoma

\*indicates that the comparison between groups is statistically significant, \* $P < 0.05$

**Fig. 2** SCEL inhibits proliferation of OSCC in vitro and in vivo. **A, B** The transfection of SCEL in OSCC cell lines was validated by qRT-PCR and Western blot, respectively. **C, D** Proliferation and colony formation assays. **E** The effect of SCEL overexpression on OSCC proliferation in vivo. **F** Comparison of SCEL and Ki-67 in different tumor tissues

### 3.3 Diagnostic efficacy of SCEL expression level in OSCC

According to the TCGA database, the AUC value of SCEL expression is 0.7455 (Fig. 1J). We performed calculations and constructed the ROC curve based on the IHC staining score for SCEL in OSCC and adjacent tissues. The AUC value for SCEL protein was found to be 0.8940 (Fig. 1K).

### 3.4 SCEL inhibited the proliferation of OSCC both in vitro and in vivo

To investigate the role of SCEL in OSCC development, we transfected OSCC cell lines with a plasmid encoding the SCEL gene and confirmed SCEL overexpression by qRT-PCR and WB analysis (Fig. 2A, B, all  $P < 0.05$ ).

The proliferation rate of OSCC cells was measured using the CCK-8 assay and colony formation assay. The CCK-8 assay showed that SCEL-overexpressing cells had significantly lower cell numbers compared to control group cells (Fig. 2C, both  $P < 0.01$ ). The colony formation assay also demonstrated a significant reduction in the number of colonies formed by SCEL-overexpressing cells compared to the control group. For CAL27 cells, the number of colonies in the SCEL-overexpressing group decreased by approximately 55.59% compared to the control group ( $P < 0.01$ ). For SAS cells, the number of colonies in the SCEL-overexpressing group decreased by approximately 47.52% compared to the control group ( $P < 0.05$ ) (Fig. 2D).

To further validate this finding, we conducted in vivo experiments using a nude mouse model. We observed a significant deceleration in tumor growth and a reduction in tumor weight in the SCEL-overexpression group compared to the vector group (Fig. 2E, both  $P < 0.05$ ). IHC staining subsequently confirmed increased SCEL expression levels in the SCEL-overexpression group. Conversely, Ki-67 staining, an indicator of proliferation, exhibited an opposite trend (Fig. 2F,  $P < 0.05$ ).

### 3.5 SCEL induces apoptosis, cell cycle arrest, and ROS production

The intricate relationship between cell proliferation and apoptosis often entails an inverse correlation, where increased proliferation is frequently accompanied by reduced apoptosis [19]. Anti-proliferative effects are frequently achieved through the induction of apoptosis. To elucidate the mechanism by which SCEL inhibits OSCC proliferation, we examined its effect on cell apoptosis by flow cytometry. As depicted in Fig. 3A, we found that SCEL significantly induced apoptosis in OSCC cells. In CAL27 cells, the total apoptosis rate increased by 12.60% in the SCEL overexpression group compared to the control group, with early apoptosis rates increasing by 12.50% and late apoptosis rates increasing by 2.55% (Fig. 3A, all  $P < 0.05$ ). In SAS cells, the total apoptosis rate increased by 19.69% in the SCEL overexpression group compared to the control group ( $P < 0.05$ ), with early apoptosis rates increasing by 18.88% (Fig. 3A, both  $P < 0.05$ ). There was no significant difference in late apoptosis rates between the two groups, although the SCEL overexpression group showed a higher trend. To understand the mechanism by which SCEL induces apoptosis, we analyzed the expression of apoptosis-related proteins. We found that the changes in proteins associated with the mitochondrial pathway were the most significant. We found that SCEL overexpression led to an increase in cleaved Caspase-9 and in BAX (Fig. 3B, all  $P < 0.05$ ).

To further investigate the mechanism by which SCEL inhibits OSCC proliferation, we examined its effect on the cell cycle. Our investigation revealed that in the SCEL overexpression group, the proportion of cells in the G1 phase significantly decreased, while the proportions of cells in the S and G2 phases increased (Fig. 3C). Specifically, in CAL27 cells, the G1 phase cell proportion in the SCEL overexpression group decreased by 11.74% compared to the control group, the S phase cell proportion increased by 4.7%, and the G2 phase cell proportion increased by 6.71% (all  $P < 0.05$ ). In SAS cells, the G1 phase cell proportion in the SCEL overexpression group decreased by 18.48%, and the S phase cell proportion increased by 15.4% (both  $P < 0.05$ ); the G2 phase cell proportion increased by 3.08%, showing an increasing trend without significant difference. Given the pivotal role of CDKs in regulating cell cycle progression and apoptosis, we examined the expression levels of related cell cycle proteins to further understand the impact of SCEL on the OSCC cell cycle. The expression levels of CDK1, CDK2, Cyclin A2, and Cyclin B1 increased, while Cyclin D1 decreased in SCEL-overexpressing



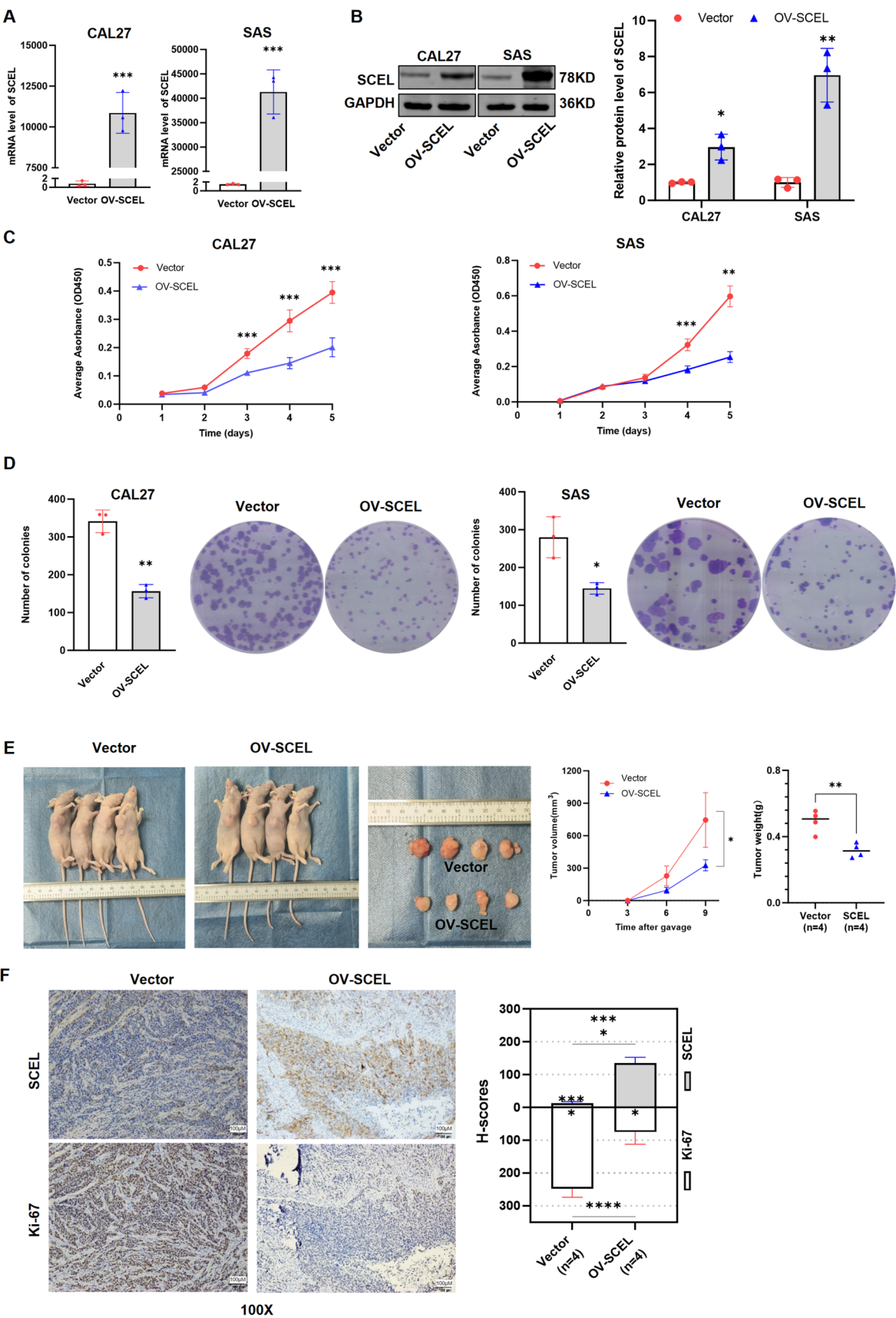


**Fig. 3** SCEL induces apoptosis, cell cycle arrest, and ROS production. **A** Analysis of apoptosis in SCEL-overexpressing OSCC cells by flow cytometry. **B** Impact of SCEL on apoptosis-related proteins in OSCC cells. **C** Analysis of cell cycle arrest in SCEL-overexpressing OSCC cells by flow cytometry. **D** Impact of SCEL on cell cycle-related proteins in OSCC cells. **E–G** Role of ROS formation in SCEL-induced apoptosis

cells (Fig. 3D). These changes suggest that SCEL may regulate cell cycle progression by causing cells to be arrested in the S and G2/M phases.

ROS can induce oxidative stress, leading to mitochondrial damage and cell death [20]. We examined the effect SCEL on ROS levels. Flow cytometry results (Fig. 3E) showed that in CAL27 cells, the ROS levels in the SCEL overexpression group increased by an average of 32.70% compared to the control group ( $P < 0.001$ ). In SAS cells, the ROS levels in the SCEL overexpression group increased by an average of 42.43% compared to the control group ( $P < 0.0001$ ). Confocal microscopy results (Fig. 3F) showed a significant increase in the fluorescence signal of ROS in the SCEL-overexpressing cells. In contrast, the ROS fluorescence signal was weaker in the control group. The mean fluorescence intensity (MFI) was increased by 19.50 times in CAL27 cells and by 13.83 times in SAS cells in the SCEL-overexpressing group compared to the control group (both  $P < 0.001$ ). Microplate reader results showed that SCEL overexpression significantly increased ROS levels, with the ROS level in CAL27 cells increasing by 1.58 times and in SAS cells by 2.59 times compared to the control group (Fig. 3G, both  $P < 0.0001$ ).

### 3.6 SCEL inhibits OSCC migration and invasion via impeding TGF- $\beta$ /Smad-EMT

To investigate the effect of SCEL on the migration and invasion abilities of OSCC cells, we conducted wound healing and Transwell chamber assays. SCEL-transfected CAL27 cells showed a reduction in migration rate by approximately 30% (Fig. 4A,  $P < 0.001$ ), while SAS cells showed a reduction by approximately 48% (Fig. 4A,  $P < 0.001$ ). Transwell chamber assays demonstrated that the invasion capacity of SCEL-transfected CAL27 cells was reduced by approximately 62% (Fig. 4B,  $P < 0.001$ ), and SAS cells by approximately 47% (Fig. 4B,  $P < 0.001$ ). These results indicate that SCEL overexpression inhibits the migration and invasion of OSCC cells.

Cell migration and invasion are driven by the EMT process. During EMT, cells transition from an epithelial phenotype to a mesenchymal phenotype by altering the expression of specific markers. We further investigated the impact of SCEL on EMT-related markers. SCEL overexpression led to an increase in epithelial markers E-cadherin and Occludin-1, while decreasing mesenchymal markers N-cadherin and Vimentin. Additionally, SCEL overexpression significantly reduced the expression of EMT transcription factors Snail and Slug. Furthermore, proteins involved in cell adhesion and signal transduction, such as  $\beta$ -Catenin and Claudin, were increased (Fig. 4C,  $P < 0.05$ ). Our results suggest that SCEL inhibits the EMT process, thereby further suppressing the migration and invasion of OSCC cells.

TGF- $\beta$  is an activator of EMT and can influence the EMT process through various pathways, but it primarily regulates key EMT transcription factors such as Snail and Slug via the TGF- $\beta$ /Smad signaling pathway [21]. We found that overexpression of SCEL significantly inhibited the expression of TGF- $\beta$ 1, SMAD2, SMAD3, and SMAD4. This suggests that SCEL may suppress the EMT process by inhibiting the TGF- $\beta$ /Smad signaling pathway, thereby reducing the migration and invasion capabilities of OSCC cells (Fig. 4D,  $P < 0.05$ ).

### 3.7 SCEL reduces lymph node metastasis in OSCC via VEGFC regulation

Lymph node metastasis is a critical outcome of cancer cell invasion and migration. Our studies have shown that the lymph node metastasis marker VEGFC is negatively correlated with SCEL expression during cancer progression (Fig. 1H, I), suggesting that SCEL may play a role in lymph node metastasis. Studies have also demonstrated that TGF- $\beta$ 1 signaling induces VEGFC expression through both Smad-dependent and Smad-independent pathways, promoting lymphangiogenesis and lymph node metastasis in gastric cancer [22]. Based on these findings, we investigated the effects of SCEL overexpression on TGF- $\beta$ 1 and VEGFC expression to explore its mechanism in inhibiting OSCC lymph node metastasis. In OSCC tissues with lymph node metastasis, SCEL expression was significantly lower (median H-score 50, 0–210) and negatively correlated with TGF- $\beta$ 1 expression compared to tissues without metastasis (median H-score 85, 0–195) (Fig. 4E,  $P < 0.05$ ). Our study demonstrated a positive correlation between mRNA levels of TGF- $\beta$ 1 and VEGFC in OSCC cells based on the analysis of the TCGA database (Fig. 4F,  $P < 0.0001$ ). Our PCR results showed that the mRNA expression level of VEGFC increased significantly after treating OSCC cells with TGF- $\beta$ 1 (Fig. 4G, both  $P < 0.001$ ). Additionally, overexpression of SCEL in OSCC cells led to a significant decrease in the protein levels of VEGFC and LYVE1 (Lymphatic Vessel Endothelial

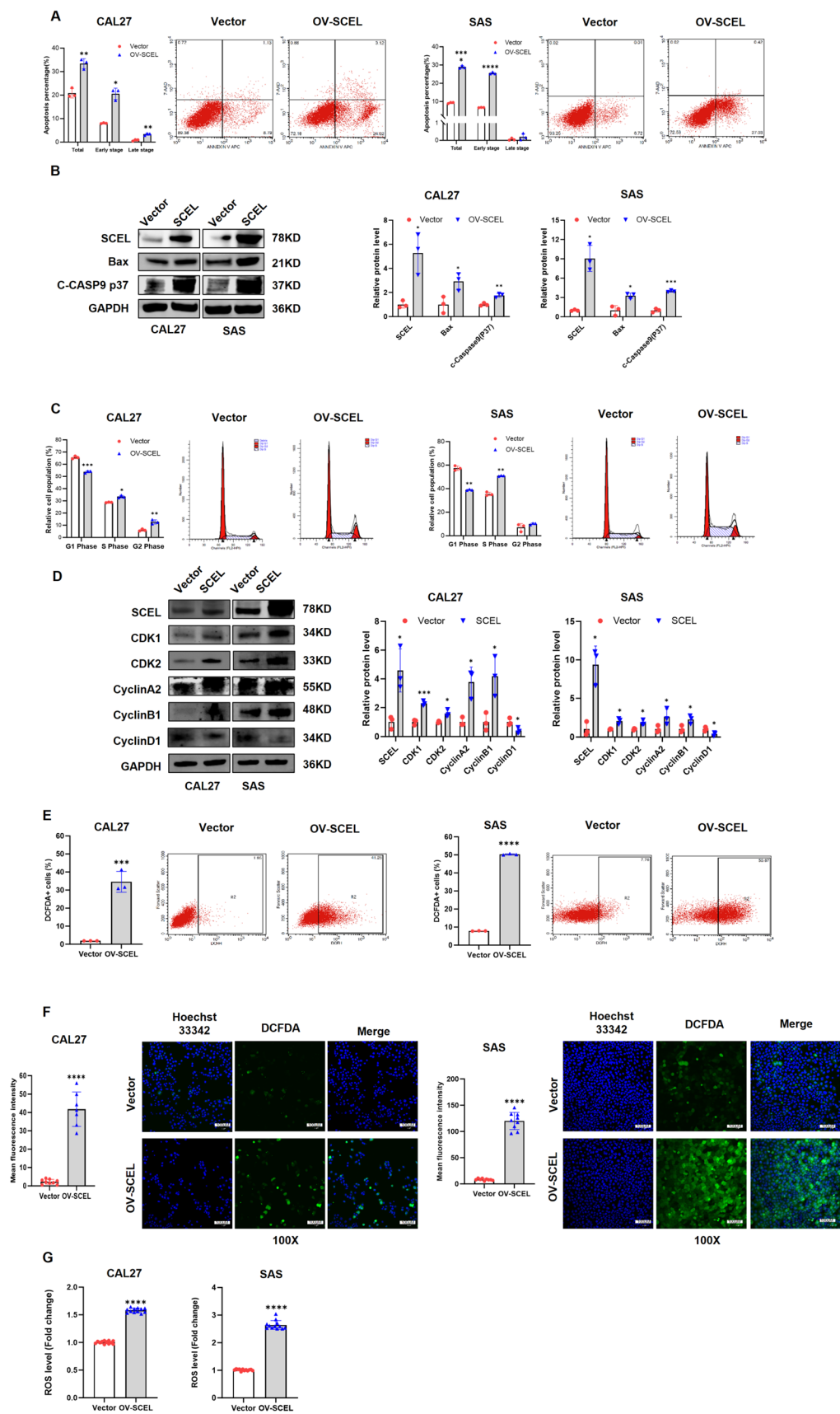


**Fig. 4** SCEL's role in OSCC progression inhibition of migration, invasion, lymph node metastasis and chemotherapy sensitivity. **A** Wound healing assay. **B** Transwell assays. **C** Western blot analysis of SCEL's effect on EMT-related protein expression. **D** Western blot analysis of SCEL's influence on the TGF- $\beta$ /Smad signaling pathway. **E** Comparison of SCEL and TGF- $\beta$ 1 expression in OSCC tissue and lymph node metastasis tissue. **F** Correlation analysis of TGF- $\beta$ 1 and VEGFC in OSCC. **G** Effect of TGF- $\beta$ 1 treatment on VEGFC production in OSCC Cells (10 ng/ml, 48 h). **H** Western blot analysis of SCEL's effect on VEGFC and LYVE1 in OSCC Cells. **I** CCK8 assay analysis of influence of SCEL on CDDP sensitivity in OSCC cells. **J** CCK8 assay analysis of SCEL on drug response in OSCC cell under low-dose CDDP treatment (4  $\mu$ M CDDP for 24 h)

Hyaluronan Receptor 1) (Fig. 4H,  $P < 0.05$ ). These results suggest that SCEL may influence lymph node metastasis by inhibiting TGF- $\beta$ 1-induced VEGFC expression.

### 3.8 SCEL enhances chemotherapy sensitivity in OSCC

In addition to inhibiting OSCC progression, SCEL also plays an important role in cancer cell sensitivity to chemotherapy. CDDP is a commonly used chemotherapy drug for OSCC treatment, but tumor cells often develop resistance to it [23]. Our study found that SCEL overexpression significantly enhanced OSCC cell sensitivity to CDDP (Fig. 4I). Specifically, in the IC<sub>50</sub> assay, the SCEL-expressing SAS cells (9.98  $\mu$ M) showed higher drug sensitivity compared to the vector group (5.96  $\mu$ M). After treatment with 4  $\mu$ M CDDP (the lowest concentration that significantly inhibits cell viability) for 24 h, the viability of vector group cells was 79.19%, while the cell viability in the SCEL overexpression group significantly decreased to 20.06% (Fig. 4J,  $P < 0.0001$ ). These results indicate that SCEL overexpression significantly enhances OSCC cell sensitivity to CDDP.

### 3.9 Overexpressing mir-5696 silences SCEL expression and promotes proliferation and invasion of OSCC

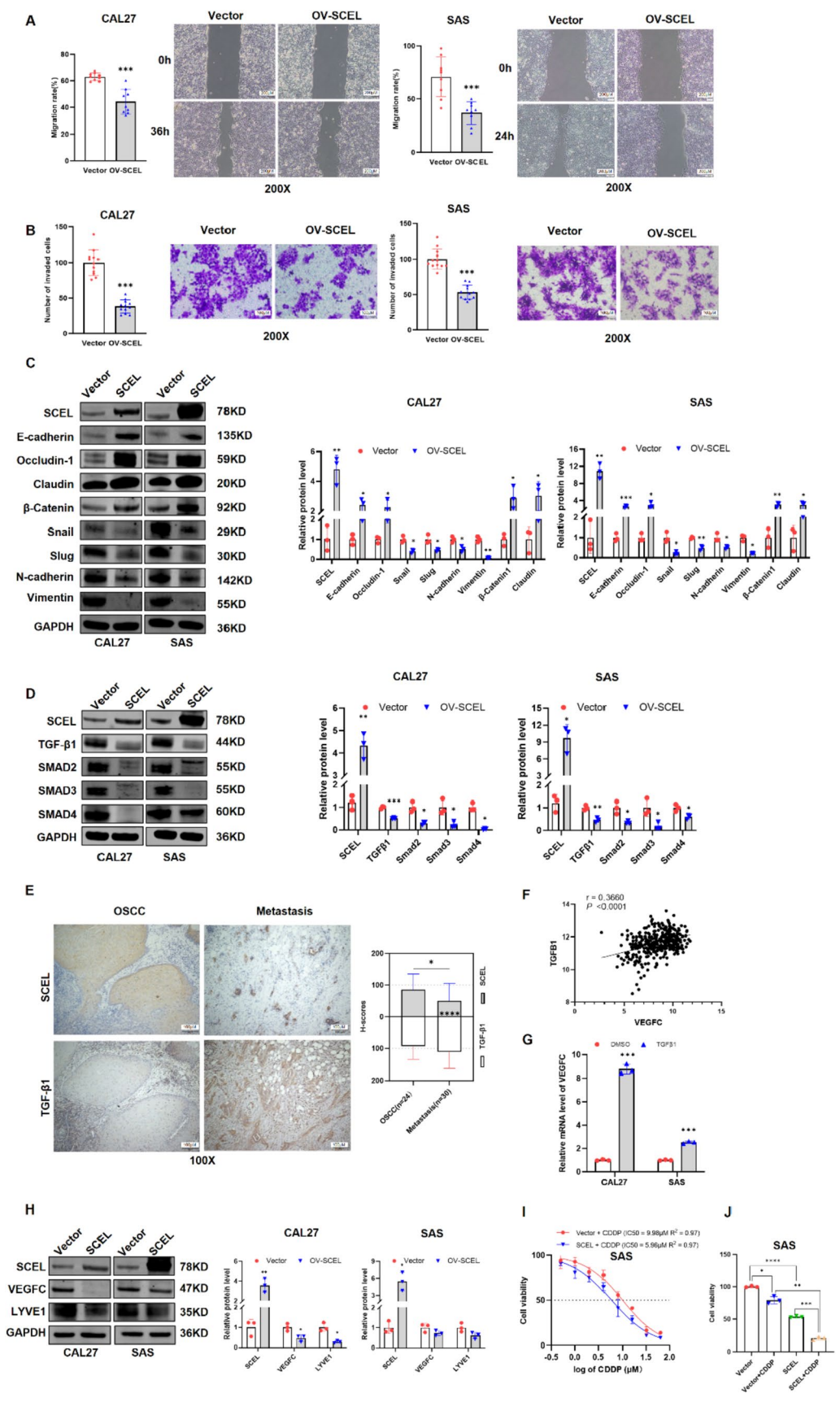
We have demonstrated that SCEL impedes the malignant biological behavior of OSCC cells. However, the molecular mechanisms underlying the abnormal inactivation of SCEL in OSCC remain unclear. MicroRNAs are non-coding RNAs that regulate post-transcriptional gene expression by binding to the 3'UTR of target genes, thereby inhibiting mRNA translation or promoting its degradation. Using four online prediction tools—Targetscan, Targets, Micro-CDS, and miRDB—we identified miR-5696 as a potential miRNA targeting SCEL (Fig. 5A). We observed that miR-5696 is highly expressed in OSCC cells and tissues (Fig. 5B, C, all  $P < 0.05$ ), displaying a negative correlation with SCEL expression (Fig. 5D,  $P < 0.05$ ). Additionally, miR-5696 mimics significantly reduced SCEL mRNA and protein levels (both  $P < 0.05$ ). Although miR-5696 inhibitor significantly increased SCEL mRNA levels ( $P < 0.05$ ), the change in protein levels exhibited an increasing trend but was not statistically significant ( $P > 0.05$ ) (Fig. 5E, F). We also predicted the miR-5696 binding sites on SCEL and constructed wild-type and mutant SCEL dual-luciferase reporter plasmids (Fig. 5G, H). The relative light units were significantly reduced in the wild-type SCEL plasmid group ( $P < 0.01$ ), whereas no significant changes were observed in the empty vector and mutant SCEL plasmid groups ( $P > 0.05$ ). This indicates that miR-5696 effectively binds to SCEL, thereby suppressing its expression. We further analyzed the impact of miR-5696 on the malignant behavior of OSCC cells. The CCK-8 assay demonstrated that overexpression of miR-5696 mimics enhanced cell proliferation, while inhibitors of miR-5696 reversed this trend (Fig. 5I, all  $P < 0.05$ ). The transwell assay showed that overexpression of miR-5696 mimics increased cell invasion, while inhibitors of miR-5696 similarly reversed this trend (Fig. 5J, all  $P < 0.0001$ ). These results suggest that the inactivation of SCEL expression may be associated with the targeted silencing by miR-5696, leading to the failure of SCEL's upstream activation system and consequently promoting the development of OSCC.

## 4 Discussion

Cancer develops by a multistep process that progressively transforms normal cells into highly malignant proliferators that pose a threat to human health [24]. Under normal physiological conditions, a delicate balance is maintained between cell differentiation and proliferation to ensure tissue homeostasis. However, in cancer, this balance is disrupted. Cancer cells typically exhibit abnormal proliferative capacity while their differentiation ability is inhibited [25]. Additionally, poorly differentiated tumor cells often have increased migratory and invasive potential [26]. Our research indicates that SCEL levels progressively decrease from normal tissue to precancerous lesions and cancer progression. This suggests that the inactivation or downregulation of SCEL may play a crucial role in promoting oral cancer development.

SCEL has been reported to be closely associated with the activation of terminal differentiation markers in the epidermis [7, 27]. SCEL's loss may lead to the cells losing their normal differentiation capacity, thereby promoting tumor progression





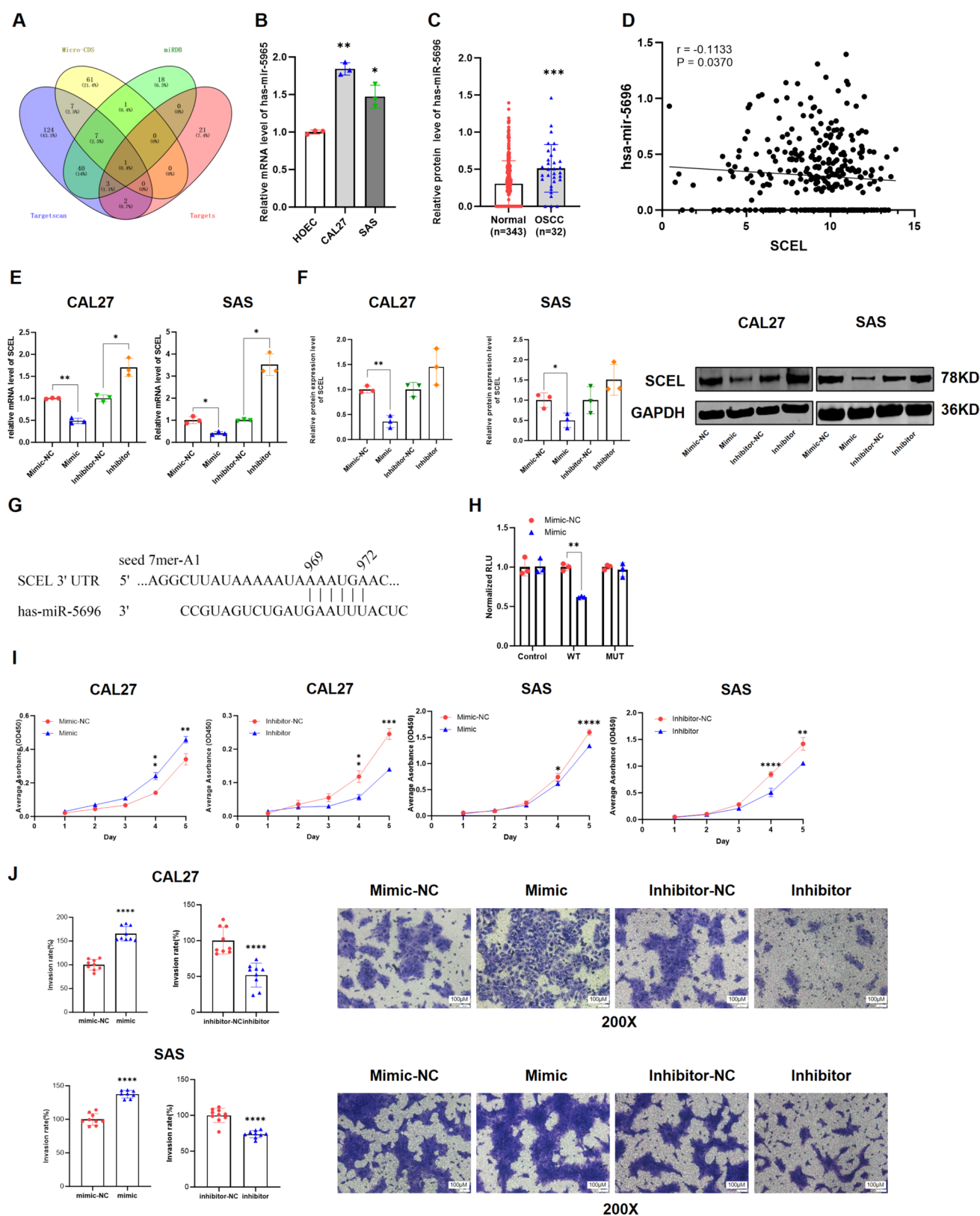


**Fig. 5** Identification and validation of has-miR-5966 targeting SCEL in OSCC. **A** miRNAs predicted by different applications for targeting SCEL. **B, C** Expression of has-miR-5966 in OSCC cells and tissues. **D** Correlation between has-miR-5966 and SCEL expression in OSCC. **E, F** Effect of has-miR-5966 mimic and inhibitor on SCEL mRNA and protein Levels. **G** Prediction of miR-5966 binding sites on SCEL. **H** Dual-Luciferase reporter assay to validate has-miR-5966 binding to SCEL. **I** CCK-8 Assay. **J** Transwell assay



[28–30]. Our study indicates that SCEL plays a crucial role in regulating the differentiation of OSCC cells. Low expression of SCEL may lead to a decrease in differentiation capacity, potentially enhancing their proliferative potential. Functional experiments further support this view, showing that SCEL significantly inhibits OSCC cell proliferation by inducing apoptosis and causing cell cycle arrest. Further research indicates that SCEL induces oxidative stress by increasing ROS levels, which may be a key mechanism for its pro-apoptotic effects.

SCEL is also closely associated with the invasive and metastatic potential of cells. SCEL reduces OSCC cell migration and invasion by inhibiting the TGF- $\beta$ /Smad-mediated EMT pathway [31], which further underscores its importance in halting tumor progression. The TGF- $\beta$ /Smad pathway is influenced by various post-translational regulatory mechanisms such as ubiquitination and phosphorylation [32]. Ubiquitination regulates the TGF- $\beta$  signaling pathway by tagging specific proteins for proteasomal degradation [33] while phosphorylation affecting the activity and stability of Smad protein [34]. These potential regulatory mechanisms merit further investigation. Additionally, SCEL expression was notably decreased in lymph node metastasis tissues. This reduction in SCEL expression may influence VEGFC levels, potentially contributing to the metastatic process and impacting patient prognosis.

Furthermore, miR-5696 plays a significant role in regulating SCEL expression. Our study found that miR-5696 can downregulate SCEL expression, thereby affecting the biological behavior of OSCC cells. However, it is important to note that while our study primarily focuses on the post-transcriptional regulation of SCEL by microRNA-5696, the inactivation of tumor suppressor genes (TSGs) in OSCC can involve a range of mechanisms, including DNA methylation and chromatin remodeling [23, 35]. This remains a significant limitation of our study, as we have not fully explored the complex interplay of these epigenetic and post-transcriptional mechanisms in TSG regulation within OSCC.

## 5 Conclusion

SCEL is significantly downregulated in OSCC cell lines and tissues, and its low expression is closely associated with decreased tumor cell differentiation and increased lymph node metastasis. SCEL inhibits OSCC proliferation and metastasis through multiple mechanisms, indicating its potential as a therapeutic target for OSCC.

**Author contributions** Danping Li: Conceptualization, Data curation, Methodology, Resources, Validation, Writing – original draft. Limei Li and Qiaoli Chen: Visualization. ShuWu: Data curation. JunZhao and Haishan Zhang: Investigation. Liudmila Matskova: Validation. Yingxi Mo: Formal analysis. Ping Li: Funding acquisition. Xiaoying Zhou: Conceptualization, Project administration, Supervision, Writing – review & editing. All authors read and approved the final manuscript.

**Funding** This work was supported by Guangxi Natural Science Foundation (2023GXNSFAA026256, 2023).

**Data availability** The datasets used and/or analyzed during the current study are available from the corresponding author on reasonable request.

## Declarations

**Ethics approval and consent to participate** The research was approved by the Institutional Review Board (IRB) at the Ethics Committee of Guangxi Medical University (No. 202004003) and conducted in accordance with the ARRIVE guidelines. The maximal allowed tumor size for this study was 1.5 cm in diameter, or a tumor burden equivalent to 10% of the total body weight of the animal. Throughout the study, tumor size and burden were carefully monitored, and it is confirmed that the maximal tumor size or burden was not exceeded in any of the animals. Human studies were performed following the Declaration of Helsinki, and ethical approval for human subjects was granted under protocol No. 2021028.

**Informed consent** Informed consents were obtained from all participants, covering both participation in the study and publication of the data.

**Competing interests** The authors declare no competing interests.

**Open Access** This article is licensed under a Creative Commons Attribution-NonCommercial-NoDerivatives 4.0 International License, which permits any non-commercial use, sharing, distribution and reproduction in any medium or format, as long as you give appropriate credit to the original author(s) and the source, provide a link to the Creative Commons licence, and indicate if you modified the licensed material. You do not have permission under this licence to share adapted material derived from this article or parts of it. The images or other third party material in this article are included in the article's Creative Commons licence, unless indicated otherwise in a credit line to the material. If material is not included in the article's Creative Commons licence and your intended use is not permitted by statutory regulation or exceeds

the permitted use, you will need to obtain permission directly from the copyright holder. To view a copy of this licence, visit <http://creativecommons.org/licenses/by-nc-nd/4.0/>.

## References

1. Rivera C. Essentials of oral cancer. *Int J Clin Exp Pathol*. 2015;8(9):11884–94.
2. González-Moles M, Aguilar-Ruiz M, Ramos-García P. Challenges in the early diagnosis of oral cancer, evidence gaps and strategies for improvement: a scoping review of systematic reviews. *Cancers (Basel)*. 2022. <https://doi.org/10.3390/cancers14194967>.
3. Chi AC, Day TA, Neville BW. Oral cavity and oropharyngeal squamous cell carcinoma—an update. *CA Cancer J Clin*. 2015;65(5):401–21. <https://doi.org/10.3322/caac.21293>.
4. Lop J, Rigó A, Codina A, et al. Prognostic significance of extranodal extension in head and neck squamous cell carcinoma cN0 patients with occult metastatic neck nodes. *Acta Otorrinolaringol Esp (Engl Ed)*. 2018;69(3):156–64. <https://doi.org/10.1016/j.otorri.2017.07.002>.
5. Epstein JB, Thariat J, Bensadoun RJ, et al. Oral complications of cancer and cancer therapy: from cancer treatment to survivorship. *CA Cancer J Clin*. 2012;62(6):400–22. <https://doi.org/10.3322/caac.21157>.
6. Zanoni DK, Montero PH, Migliacci JC, et al. Survival outcomes after treatment of cancer of the oral cavity (1985–2015). *Oral Oncol*. 2019;90:115–21. <https://doi.org/10.1016/j.oraloncology.2019.02.001>.
7. Champiaud MF, Burgeson RE, Jin W, et al. cDNA cloning and characterization of sciellin, a LIM domain protein of the keratinocyte cornified envelope. *J Biol Chem*. 1998;273(47):31547–54. <https://doi.org/10.1074/jbc.273.47.31547>.
8. Kvedar JC, Manabe M, Phillips SB, et al. Characterization of sciellin, a precursor to the cornified envelope of human keratinocytes. *Differentiation*. 1992;49(3):195–204. <https://doi.org/10.1111/j.1432-0436.1992.tb00667.x>.
9. Chou CK, Fan CC, Lin PS, et al. Sciellin mediates mesenchymal-to-epithelial transition in colorectal cancer hepatic metastasis. *Oncotarget*. 2016;7(18):25742–54. <https://doi.org/10.18632/oncotarget.8264>.
10. Li Y, Yuan R, Ren T, et al. Role of Sciellin in gallbladder cancer proliferation and formation of neutrophil extracellular traps. *Cell Death Dis*. 2021;12(1):30. <https://doi.org/10.1038/s41419-020-03286-z>.
11. Xu J, Lamouille S, Derynck R. TGF-beta-induced epithelial to mesenchymal transition. *Cell Res*. 2009;19(2):156–72. <https://doi.org/10.1038/cr.2009.5>.
12. Nair J, Jain P, Chandola U, et al. Gene and miRNA expression changes in squamous cell carcinoma of larynx and hypopharynx. *Genes Cancer*. 2015;6(7–8):328–40. <https://doi.org/10.18632/genesandcancer.69>.
13. Zhao X, Sun S, Zeng X, et al. Expression profiles analysis identifies a novel three-mRNA signature to predict overall survival in oral squamous cell carcinoma. *Am J Cancer Res*. 2018;8(3):450–61.
14. Yang YF, Chang YC, Tsai KW, et al. UBE2C triggers HIF-1α-glycolytic flux in head and neck squamous cell carcinoma. *J Cell Mol Med*. 2022;26(13):3716–25. <https://doi.org/10.1111/jcmm.17400>.
15. Ji J, Chen J, Wang A, et al. KK-LC-1 may be an effective prognostic biomarker for gastric cancer. *BMC Cancer*. 2021;21(1):267. <https://doi.org/10.1186/s12885-021-07974-7>.
16. Bi Y, Shi X, Chen D, et al. CD133, but not CD44, may serve as a novel biomarker for differential diagnosis between basal cell carcinoma and trichoblastomas. *Clin Cosmet Investig Dermatol*. 2022;15:1517–26. <https://doi.org/10.2147/ccid.S373331>.
17. Truong AB, Kretz M, Ridky TW, et al. p63 regulates proliferation and differentiation of developmentally mature keratinocytes. *Genes Dev*. 2006;20(22):3185–97. <https://doi.org/10.1101/gad.1463206>.
18. Li X, Liu B, Xiao J, et al. Roles of VEGF-C and Smad4 in the lymphangiogenesis, lymphatic metastasis, and prognosis in colon cancer. *J Gastrointest Surg*. 2011;15(11):2001–10. <https://doi.org/10.1007/s11605-011-1627-2>.
19. Morana O, Wood W, Gregory CD. The Apoptosis Paradox in Cancer. *Int J Mol Sci*. 2022. <https://doi.org/10.3390/ijms23031328>.
20. Moloney JN, Cotter TG. ROS signalling in the biology of cancer. *Semin Cell Dev Biol*. 2018;80:50–64. <https://doi.org/10.1016/j.semcdb.2017.05.023>.
21. Gonzalez DM, Medici D. Signaling mechanisms of the epithelial-mesenchymal transition. *Sci Signal*. 2014;7(344):re8. <https://doi.org/10.1126/scisignal.2005189>.
22. Åström P, Juurikka K, Hadler-Olsen ES, et al. The interplay of matrix metalloproteinase-8, transforming growth factor-β1 and vascular endothelial growth factor-C cooperatively contributes to the aggressiveness of oral tongue squamous cell carcinoma. *Br J Cancer*. 2017;117(7):1007–16. <https://doi.org/10.1038/bjc.2017.249>.
23. Oh SY, Kim J, Lee KY, et al. Chromatin remodeling-driven autophagy activation induces cisplatin resistance in oral squamous cell carcinoma. *Cell Death Dis*. 2024;15(8):589. <https://doi.org/10.1038/s41419-024-06975-1>.
24. Hanahan D, Weinberg RA. The hallmarks of cancer. *Cell*. 2000;100(1):57–70. [https://doi.org/10.1016/s0092-8674\(00\)81683-9](https://doi.org/10.1016/s0092-8674(00)81683-9).
25. Jetten AM, Harvat BL. Epidermal differentiation and squamous metaplasia: from stem cell to cell death. *J Dermatol*. 1997;24(11):711–25. <https://doi.org/10.1111/j.1346-8138.1997.tb02523.x>.
26. Wang H, Unteraehrer JJ. Epithelial-mesenchymal transition and cancer stem cells: at the crossroads of differentiation and dedifferentiation. *Dev Dyn*. 2019;248(1):10–20. <https://doi.org/10.1002/dvdy.24678>.
27. Champiaud MF, Baden HP, Koch M, et al. Gene characterization of sciellin (SCEL) and protein localization in vertebrate epithelia displaying barrier properties. *Genomics*. 2000;70(2):264–8. <https://doi.org/10.1006/geno.2000.6390>.
28. Mehrel T, Hohl D, Rothnagel JA, et al. Identification of a major keratinocyte cell envelope protein, loricrin. *Cell*. 1990;61(6):1103–12. [https://doi.org/10.1016/0092-8674\(90\)90073-n](https://doi.org/10.1016/0092-8674(90)90073-n).
29. Tesfagzi J, Carlson DM. Expression, regulation, and function of the SPR family of proteins. A review. *Cell Biochem Biophys*. 1999;30(2):243–65. <https://doi.org/10.1007/bf02738069>.
30. Janes SM, Ofstad TA, Campbell DH, et al. Transient activation of FOXN1 in keratinocytes induces a transcriptional programme that promotes terminal differentiation: contrasting roles of FOXN1 and Akt. *J Cell Sci*. 2004;117(Pt 18):4157–68. <https://doi.org/10.1242/jcs.01302>.

31. Mittal V. Epithelial mesenchymal transition in tumor metastasis. *Annu Rev Pathol.* 2018;13:395–412. <https://doi.org/10.1146/annurev-pathol-020117-043854>.
32. Xu P, Liu J, Derynck R. Post-translational regulation of TGF- $\beta$  receptor and Smad signaling. *FEBS Lett.* 2012;586(14):1871–84. <https://doi.org/10.1016/j.febslet.2012.05.010>.
33. Sinha A, Iyengar PV, Ten Dijke P. E3 ubiquitin ligases: key regulators of TGF $\beta$  signaling in cancer progression. *Int J Mol Sci.* 2021. <https://doi.org/10.3390/ijms22020476>.
34. Li J, Zou Y, Kantapan J, et al. TGF- $\beta$ /Smad signaling in chronic kidney disease: exploring post-translational regulatory perspectives (review). *Mol Med Rep.* 2024. <https://doi.org/10.3892/mmr.2024.13267>.
35. Kim SY, Han YK, Song JM, et al. Aberrantly hypermethylated tumor suppressor genes were identified in oral squamous cell carcinoma (OSCC). *Clin Epigenetics.* 2019;11(1):116. <https://doi.org/10.1186/s13148-019-0715-0>.

**Publisher's Note** Springer Nature remains neutral with regard to jurisdictional claims in published maps and institutional affiliations.